Appl. Phys. A (2017) 123:672
DOI 10.1007/s00339-017-1285-7

Applied Physics A
Materials Science & Processing

Geometry and near-field coupling effects on the refractive-index sensitivities of individual Ag nanoparticle sensors

Sheng Peng[1] · ChaoLing Du[1] · DaNing Shi[1]

Received: 14 June 2017 / Accepted: 19 September 2017 / Published online: 6 October 2017

Abstract The refractive-index sensitivities of sensors of individual Ag nanoparticles (including nanodisks, nanocubes, and nanoprisms) and nanoparticle clusters are investigated numerically and analytically. It is demonstrated that the refractive-index sensitivities are a nonlinear function of the peak positions of localized surface plasmon resonances (LSPRs) with fixed surrounding mediums and metal materials at optical wavelengths. Moreover, this nonlinear function is independent of Ag nanoparticle geometries and near-field couplings between components within nanoparticle clusters. In addition, the discrepancies between our results and those of literatures are also discussed. The present work facilitates choosing appropriate peak positions of LSPRs for plasmonic sensing and detections by only analytically calculating with an equation under LSPR condition.

Keywords Localized surface plasmon resonance · Plasmonic sensors · Refractive index sensitivity · Discrete dipole approximation

1 Introduction

Noble metal nanoparticles support localized surface plasmon resonances (LSPRs) at optical wavelengths, which peak positions are noticed to be greatly sensitive to the refractive index (RI) of their surrounding mediums [1–4]. This serves as the base for their rich applications in optical and bio/chemical sensing and detections [5–17]. Therein, the RI sensitivity S has been defined as the ratio of shifts in the corresponding LSPRs, normally the dipolar LSPRs, peak positions (λ_{LSPR}) to changes in the RI (n_m) of the nanoparticles' surrounding mediums.

Recently, investigations to explore what parameters controlling the RI sensitivities of plasmonic sensors have attracted increasing attentions [5–10]. By a quasi-static approximation, the RI sensitivities of Au nanowires have been analytically demonstrated to be governed only by λ_{LSPR} once the RI of their surrounding mediums is fixed [9]. That is, the function of S (vs. λ_{LSPR}) is independent of the detailed nanowire geometries, including nanowire cross-sections, sizes, and shapes. Then, this is able to extend to individual Ag nanoparticle sensors, which is interesting to be clarified. It is promising for their applications in sensing and detections, where only appropriate λ_{LSPR} needs to be considered regardless of nanoparticles' detailed geometries. In addition, near-field coupling effects between components within nanoparticle clusters on S have not been reported to the best of our knowledge. It is significant for their future plasmonic sensor designing and applications while numerical calculation provides an efficient way to deliver this. Meanwhile, the changing tendency of S with λ_{LSPR} is revealed to be linear or nonlinear, even at the same wavelength range [5–9]. Moreover, an inflexion has been observed for S at ~800 or 1000 nm for some Ag nanoparticles in experiment [7, 8], which also needs to be confirmed and/or explained, from theoretical point of view.

Therefore, in this paper, the geometry of individual Ag nanoparticles (including nanodisks, nanocubes, and nanoprisms) and near-field couplings between components within Ag nanoparticle clusters on the relationship between S and λ_{LSPR} are numerically investigated by discrete dipole approximation (DDA) [18–23] and finite element method (FEM)

✉ ChaoLing Du
cldu@nuaa.edu.cn

[1] College of Science, Nanjing University of Aeronautics and Astronautics, Nanjing 211100, People's Republic of China

[24]. It is revealed that the geometry and near-field couplings do not affect such relationship although they affect λ_{LSPR} of Ag nanoparticle sensors. In addition, values of S are demonstrated to increase nonlinearly with λ_{LSPR} at our whole wavelength range considered while a nearly negligible inflexion at ~800 nm is observed. These are analytically explained well in terms of the dielectric response of the metal nanoparticle and the dipolar LSPR condition. The present work is significant for choosing appropriate exciting wavelength in plasmonic sensing/detection applications.

2 Simulation structures and methods

The dotted circle, square, and triangle in the upper insets of Fig. 1 show the schematic cross section of the concerned individual nanodisks, nanocubes and nanoprisms, respectively; three types of normally encountered nanoparticles in experiments [7, 8, 10]. Their diameters, diagonals, and triangular heights vary from 10 to 100 nm while the corresponding nanoparticle heights are kept as 5 nm, 5 and 10 nm (or 4 nm), respectively. Aspect ratios R are defined as the ratios between disk's diameter, cube's diagonal and triangular height to nanoparticle heights, respectively. The incident light is illuminated perpendicular to the text and along nanoparticles' heights. E in Fig. 1 illustrates the incident polarization direction. Then, their corresponding extinction efficiencies are calculated numerically by DDA on a cubic grid with a lattice constant 1 nm [18–23]. The complex refractive indexes of Ag are taken from experiments [26] after size correction [1]. Data of λ_{LSPR} of the concerned nanoparticles are measured from their calculated extinction spectra. Then, values of S of their λ_{LSPR} responding to the RI of surrounding mediums are obtained by $S = \frac{\lambda_{LSPR}(n_m+0.02)-\lambda_{LSPR}(n_m-0.02)}{0.04}$. Those of the dimer counterparts of the concerned nanoparticles and plane Ag nanosphere (NSP) clusters (including NSP monomers, dimers, trimers, pentamers, and heptamers) are also calculated by DDA and FEM [25, 27–30], respectively, to explore near-field coupling effects between their component nanoparticles. Herein, values of λ_{LSPR} have been limited below ~1400 nm considering the absorption limit of water and chemical/biological molecules.

3 Results and discussions

Figure 1 presents the typical extinction efficiency spectra of the concerned three types of Ag nanoparticles. It reveals that with the same aspect ratio and RI, the concerned three different nanoparticles get different spectra shapes. This originates from their different near-electromagnetic (EM)-field distributions owing to different nanoparticle shapes, which further leads to their different extinction efficiencies, then different extinction spectra shapes and λ_{LSPR}. For illustration, typical near-field ($|E|$) distributions at their corresponding λ_{LSPR} have been presented in the upper insets of Fig. 1, which are revealed to be shape dependent. The $|E|$ distributions are also nanoparticle R, hence size dependent, which contributes to the size-dependent λ_{LSPR} as shown in Fig. 2. Figure 2 demonstrates that λ_{LSPR} increases linearly with R regardless of nanoparticle shapes. The nanoprism is revealed to get the largest intercept and slope while the nanodisk gets the smallest ones. Compared with their extinction spectra at other n_m and with even larger R (results not shown), λ_{LSPR} is revealed to be RI, nanoparticle shape, and size dependent, which agrees well with reports elsewhere [7, 8, 10].

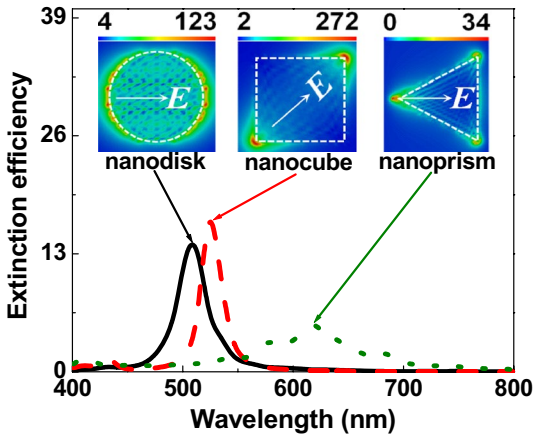

Fig. 1 Typical extinction efficiency spectra of the concerned individual Ag nanoparticle sensors with $n_m = 1.33$. Each aspect ratio and height of the three nanoparticles herein are 4 and 5 nm, respectively. The upper insets show the near-field ($|E|$) distributions at their corresponding λ_{LSPR}

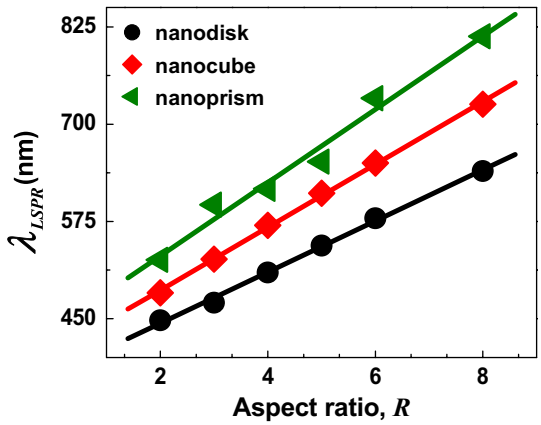

Fig. 2 Aspect ratio-dependent λ_{LSPR} of the concerned individual Ag nanoparticle sensors with $n_m = 1.33$. The solid curves present the linear fitting results

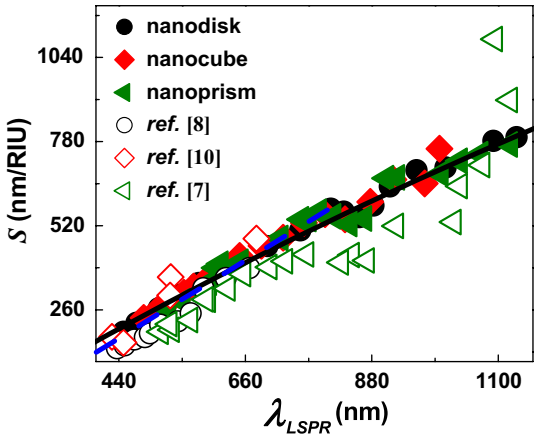

Fig. 3 The function of RI sensitivity S versus λ_{LSPR} of DDA calculated results (solid symbols), analytical results (solid curve) by Eq. 3, and those of experimental data (hollow symbols) of the concerned individual Ag nanoparticle sensors with $n_m = 1.33$. The dashed curve presents the linear fitting results

According to our DDA calculations for each type nanoparticle concerned, it demonstrates that the corresponding λ_{LSPR} is tunable from visible to infrared by the nanoparticle aspect ratios for different specific n_m. This means that at a specific n_m, values of λ_{LSPR} of the different shape nanoparticles are able to be tuned by their aspect ratios to be comparable and even equal. Then, starting from S definition and the calculated λ_{LSPR}, the RI sensitivities of the concerned nanoparticles in water are obtained and plotted as a function of their λ_{LSPR} in Fig. 3, along with their available experimental data. It shows that our DDA-calculated S of Ag nanocubes merge well with that of experimental results [10] while those of nanoprisms and nanodisks are a bit larger than their corresponding measured results [7, 8]. These discrepancies are acceptable as theoretical RI sensitivities provide upper limits for individual nanoparticle sensors while ensemble nanoparticles are normally adopted in experiments [7, 8, 10]. Figure 3 demonstrates that at nearly the same λ_{LSPR}, values of S of different shape nanoparticles are almost the same, regardless of nanoparticles' detailed geometries. This indicates that S is a function of λ_{LSPR} and the function is independent of nanoparticles' detailed geometries, such as shapes and aspect ratios, hence sizes. It agrees well with predications elsewhere for Au nanowires at optical wavelengths [9]. Figure 3 also demonstrates that S increases with λ_{LSPR} below 800 nm, but experiences an inflexion at ~800 nm, that is, S drops at ~800 nm and increases with λ_{LSPR} again from the dropping point, regardless of the nanoparticle shapes and aspect ratios. Additionally, S data in Fig. 3 below 800 nm are able to be fitted quite well both linearly and nonlinearly with the dashed and solid curves, respectively. The linearity agrees well with experiments of Charles et al. [7] and the simulations by Miller et al. [5, 6], which comes from the linear response of the real part of the dielectric functions of noble metal nanoparticles in the corresponding λ_{LSPR} range. Yet, the upper λ_{LSPR} limit of the linearity is smaller than that of Liu GL et al. (~1000 nm). Therein, only several experimental data locating at larger λ_{LSPR} than 800 nm are provided [8]. The observed drop at ~800 nm in Fig. 3 is calculated to be small. S decreases only from ~573 nm/RIU (558 and 548 nm/RIU) at 809 nm (800 and 813 nm) to ~565 nm/RIU (536, and 525 nm/RIU) at 831 nm (833 and 841 nm) for Ag nanodisks (nanocubes, and nanoprisms). The observed inflexion is verified by Charles's experimental data [7], which drops at nearly the same λ_{LSPR}. Hence, both our calculations and experimental data imply that S of individual Ag nanoparticle sensors exhibits one same function versus λ_{LSPR}.

To explore the origin of such inflexion further, we calculated the RI sensitivities of the concerned nanoparticles at $n_m = 1.60$. The results (Fig. 4) show that S increases with λ_{LSPR} till to ~800 nm, and then exhibits a small inflexion at ~800 nm. Calculations for S of individual Au nanoparticle sensors also reveal a small flexion at ~800 nm (results not shown herein). However, the value of S still shows a general increasing tendency versus λ_{LSPR} if we neglect such small inflexions. Values of S in Figs. 3 and 4 still exhibit small fluctuations around the solid curve as λ_{LSPR} deviates from the flexion point. This may come from the calculation limit as small deviation of λ_{LSPR}leads to large discrepancies of S owing to $S = \frac{\lambda_{LSPR}(n_m+0.02)-\lambda_{LSPR}(n_m-0.02)}{0.04}$. However, S data herein show good repeatability by FEM and by a different DDA user to perform the simulations. It indicates that the observed inflexion is not owing to our calculation limit as it appears regardless of the metal types, refractive indexes,

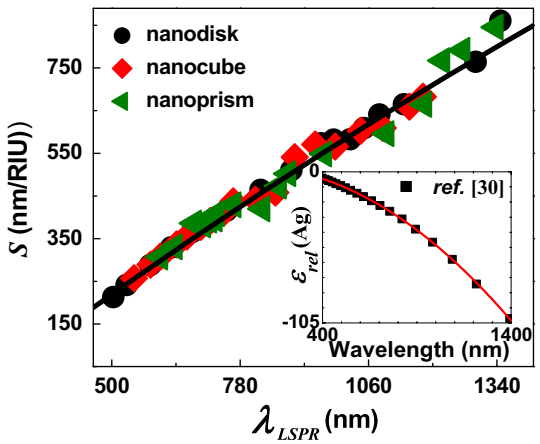

Fig. 4 The function of RI sensitivity S versus λ_{LSPR} of DDA calculated results (solid symbols), and analytical results (solid curve) by Eq. 3 of the concerned individual Ag nanoparticle sensors with $n_m = 1.60$. The lower right inset shows the quadratic fitting results (solid curve) by Eq. 1 to the experimental data of $\varepsilon_{rel}(Ag)$

and simulation methods. The inflexion position is revealed to coincide with or little larger than the starting point of infrared light. Then, it is plausible to correlate closely with the energy band structure of the concerned nanoparticles as interband absorption begins to have contributions to the dielectric responses of noble metals just from infrared light [26].

It is noted that in optical sensing and detection experiments, a general tendency of S versus λ_{LSPR} in the whole λ_{LSPR} range is preferred. This is significant to provide a theoretical guideline for their plasmonic sensor/detector designing to choose appropriate λ_{LSPR}. Therefore, we will try to develop a general nonlinear function of S (vs. λ_{LSPR}) at our concerned wavelength range while neglecting the abovementioned small fluctuations and inflexions in what follows.

We adopt the following Eq. 1 as Ref [9]. did for Au nanowires to fit the real part of Ag dielectric constant ε_{rel}.

$$\varepsilon_{rel} = A\lambda^2 + B\lambda + C \tag{1}$$

Herein, A, B and C are fitting parameters while λ is the incident light wavelength. The fitting results are shown in the lower right inset of Fig. 4, which merge well with reference data [26] and show fitting goodness larger than 99.9%. Under the dipolar LSPR condition, a shape factor of $\chi = (1-L)/2L$ is normally introduced with L being geometrical parameter. Then, we have

$$\varepsilon_{rel}|_{LSPR} = -2\chi {n_m}^2 \tag{2}$$

According to S definition [5, 6], S of individual Ag nanoparticle sensors is analytically deduced to follow Eq. 3, which has been used in Figs. 3 and 4.

$$S = \frac{d\lambda_{LSPR}}{dn_m} = \frac{1}{n_m}\left[\left(\lambda_{LSPR} + \frac{B}{2A}\right) + \frac{\frac{C}{A} - \frac{B^2}{4A^2}}{\left(\lambda_{LSPR} + \frac{B}{2A}\right)}\right] \tag{3}$$

The expression of Eq. 3 is the same as that of Au nanowires except with different fitting parameter values [26]. The good agreement of the results between our DDA calculations and Eq. 3 in Figs. 3 and 4 indicates that Eq. 3 applies to Ag nanoparticles well under dipolar LSPR condition. It demonstrates that at the whole λ_{LSPR} concerned, S is a nonlinear function of λ_{LSPR}, which is independent of the detailed nanoparticle shapes and sizes. In addition, the RI sensitivity of individual Ag nanoparticle sensors is determined only by λ_{LSPR} once the RI of surrounding mediums and metal type is fixed. Equation 3 also facilitates choosing appropriate λ_{LSPR} for plasmonic sensing/detections by analytically calculation with Eq. 3 directly. Moreover, the increasing behavior of S with λ_{LSPR} encourages researchers to get larger λ_{LSPR} to access larger S under fixed surrounding mediums.

We then employed plane Ag NSP clusters (including NSP dimers, trimers, pentamers, and heptamers) to check whether the near-field couplings between component NSPs will affect the relationship between S and λ_{LSPR}. The gap distances between components and radius of NSPs are set to 2 and 10 nm, respectively. Figure 5 presents the comparison between their numerically calculated S by FEM [25, 27] and those of analytical results by Eq. 3 along with the corresponding results of individual Ag NSP monomers [27]. Both the two dipolar LSPR modes of trimer and heptameter are presented, which have been labeled as trimer/heptameter 1 and 2 [25], respectively, in Fig. 5. Numerical results show excellent agreement with our analytical calculations by Eq. 3. It indicates that near-field couplings between component NSPs within a specific cluster sensor only has negligible effect on the relationship between S and λ_{LSPR}. The solid curve in the lower-right inset of Fig. 5 is noted to be a line. It confirms that S varies linearly with λ_{LSPR} at visible wavelengths, similar to our results of individual Ag nanodisks, nanocubes, and nanoprisms and reports elsewhere [5–7], originating from the linear response of $\varepsilon_{rel}(Ag)$. The near-field coupling independence of the quadratic coefficients of the function of λ_{LSPR} (vs. n_m) [25] may make their function of S (vs. λ_{LSPR}) be independent of such near-field couplings.

To simultaneously explore nanoparticle shape and near-field coupling effects on the relationship between S and λ_{LSPR}, the results of individual Ag dimer counterparts of our concerned three types of nanoparticles with different orientations are calculated by DDA as well. The aspect ratio of each component is set as 6, 8, and 9 (or 10) for the nanodisk, nanocube, and nanoprism dimers, respectively, while the height of each component is 5 nm for all the dimers. Different dimers with different orientations are revealed to get different λ_{LSPR}, reflecting their different near-field couplings.

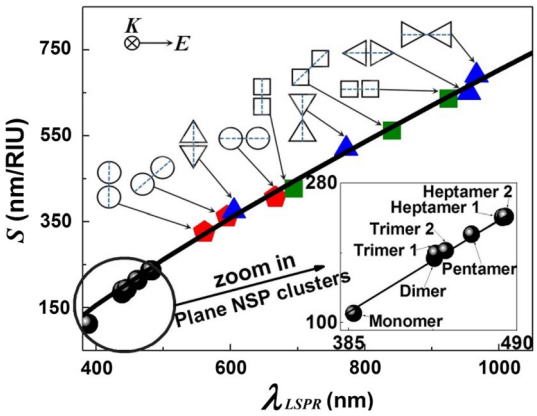

Fig. 5 The function of RI sensitivity S versus λ_{LSPR} of the calculated results (solid symbols), and analytical results (solid curve) by Eq. 3 of Ag nanoparticle cluster sensors (including plane Ag NSP clusters and dimer counterparts of the concerned three types of nanoparticles) with $n_m = 1.33$. The upper-left inset and hollow symbols show the configurations of the incident light and nanoparticle dimers, respectively

The obtained S are also plotted in Fig. 5. As expected, all the calculated data, regardless of dimer orientations and nanoparticle shapes of dimer components, fall on the same solid curve predicted by Eq. 3. It demonstrates that nanoparticle shapes, dimer orientations, and near-field couplings between components do not affect the relationship between S and λ_{LSPR}. Accordingly, the linear/quadratic response of $\varepsilon_{rel}(Ag)$ at visible/optical wavelengths contributes to the linear/nonlinear responses of S to λ_{LSPR}. The analytical developed Eq. 3 herein provides a direct and easy-to-use method to predict S of individual Ag nanoparticle sensors regardless of the detailed geometry of the sensor, and the fact that the LSPR sensor is composed by only a single nanoparticle or several neighboring nanoparticles.

4 Conclusions

In this paper, we have studied the relationship between the RI sensitivities and peak positions of LSPRs of Ag nanoparticle sensors (including individual nanoparticles and nanoparticle clusters) numerically and analytically. The relationship is demonstrated to be nonlinear, and independence of the nanoparticle geometry and near-field couplings between components within nanoparticle clusters. This originates from the quadratic response of $\varepsilon_{rel}(Ag)$ from visible to infrared wavelengths. In addition, the small inflexion of RI sensitivities at ~800 nm is revealed to come from the inter-band absorption effect of the nanoparticles. Moreover, the analytically obtained nonlinear increasing behavior of RI sensitivities encourages researchers to get larger peak positions of LSPRs to access larger RI sensitivities with fixed surrounding mediums. It is believed to hold great promise for the future development of LSPR based nano-devices for use in optical and bio/chemical sensing and detections.

Acknowledgements This work was finically supported by the Fundamental Research Funds for the Central Universities (No. NS2016074).

References

1. U. Kreibig, M. Vollmer, *Optical Properties of Metal Clusters* (Springer, Berlin, 1995)
2. C.F. Bohren, D.R. Huffman, *Absorption and Scattering of Light by Small Particles* (Wiley, New York, 1983)
3. T.R. Jensen, M.L. Duval, K.L. Kelly, A.A. Lazarides, G.C. Schatz, R.P. Van Duyne, J. Phys. Chem. B **103**, 9846–9853 (1999)
4. A.J. Haes, R.P. Van Duyne, Am. Chem. Soc. **124**, 10596–10604 (2002)
5. M.M. Miller, A.A. Lazarides, J. Phys. Chem. B **109**, 21556–21565 (2005)
6. M.M. Miller, A.A. Lazarides, J. Opt. A **8**, S239-S249 (2006)
7. D.E. Charles, D. Aherne, M. Gara, D.M. Ledwith, Y.K. Gun'ko, J.M. Kelly, W.J. Blau, M.E. Brennan-Fournet, ACS Nano. **4**, 55–64 (2010)
8. A.U. Khan, S. Zhao, G.L. Liu, J. Phys. Chem. C **120**, 19353–19364 (2016)
9. S.F. Ophélie, L. Gaëtan, B. Rabah, S. Sabine, A. Abdellatif, J. Phys. Chem. C **119**, 28551–28559 (2015)
10. N. Ahamad, A. Bottomley, A. Ianoul, J. Phys. Chem. C **116**, 185–192 (2012)
11. A.D. McFarland, R.P. Van Duyne, Nano Lett. **3**, 1057–1062 (2003)
12. P.Y. Wang, Y.J. Bai, C. Yao, Anal Chem. **89**, 2583–2591 (2017)
13. C.L. Du, C.J. Du, Y.M. You, Appl. Opt. **50**, 4922–4926 (2011)
14. A.K. Mishra, S.K. Mishra, Sens. Actuator B **237**, 969–973 (2016)
15. H. Chen, X. Kou, Z. Yang, W. Ni, J. Wang, Langmuir **24**, 5233–5237 (2008)
16. A.J. Haes, L. Chang, L.W. Klein, R.P. Van Duyne, J. Am. Chem. Soc. **127**, 2264–2271 (2005)
17. B. Sepúlveda, P.C. Angelomé, L.M. Lechuga, L.M. Liz-Marzán, Nano Today **4**, 244–251 (2009)
18. E.M. Purcell, C.R. Pennypacker, Astrophys. J. **186**, 705–714 (1973)
19. J.J. Goodman, B.T. Draine, P.J. Flatau, J. Opt. Lett. **16**, 1198–1200 (1991)
20. B.T. Draine, J.J. Goodman, Astrophys. J. **405**, 685–697 (1993)
21. P.J. Flatau, Opt. Lett. **22**, 1205–1207 (1997)
22. http://www.ddscat.org
23. M.J. Collinge, B.T. Draine, J. Opt. Soc. Am. **21**, 2023–2028 (2004)
24. http://www.comsol.com
25. C.L. Du, B.B. Wang, F. Sun, M.L. Huang, C.J. He, Y.W. Liu, X.J. Zhang, D.N. Shi, Sens. Actuators B **215**, 142–145 (2015)
26. P.B. Johnson, R.W. Christy, Phys. Rev. B **6**, 4370–4739 (1972)
27. C.L. Du, M.L. Huang, T. Chen, F. Sun, B.B. Wang, C.J. He, D.N. Shi, Sens. Actuators B **203**, 812–816 (2014)
28. Y.F. Chau, M.W. Chen, D.P. Tsai, Appl. Opt. **48**, 617–622 (2009)
29. Y.F. Chau, J.Y. Syu, C.T. Chao, H.P. Chiang, C.M. Lim, J. Phys. D **50**, 045105 (2017)
30. K. Bao, N.A. Mirtin, P. Nordlander, Appl. Phys. A **100**, 333–339 (2010)